MM Science Journal | www.mmscience.eu
ISSN 1803-1269 (Print) | ISSN 1805-0476 (Online)
Special Issue | HSM 2025
18th International Conference on High Speed Machining
October 15-16, 2025, Metz, France.
DOI: 10.17973/MMSJ.2025_11_2025147

HSM2025-45075

EARLY CHATTER DETECTION THROUGH REAL-TIME SUPERVISION AND TIME-DOMAIN SIMULATION-BASED INDICATORS

Enrique Mireles Hernandez*,[1,2], Mikhail Guskov[1], Philippe Lorong[1], Théo Dorlin[2], Habib Karaouni[2]

[1]Laboratoire PIMM, Arts et Metiers Institude of Technology, 151 boulevard de l'Hopital, 75013 Paris, France
[2]Safran S.A., Research & Technology Center, F-78772 Magny-les-Hameaux, France

Abstract

Chatter undermines surface quality, tool life, and productivity, and most available indicators react only after vibration is fully developed. We introduce a real-time monitoring framework for turning that runs short time-domain simulations, extracts a single energy-trend indicator from the tool's phase-space spiral area, and triggers threshold-based decisions. The indicator crosses its zero threshold several spindle revolutions before visible amplitude growth, enabling proactive speed or depth adjustments and extending machine life. Validation with reconstructed a literature case confirms the indicator's robustness and its ability to track the stability-lobe boundary from one kinematic signal.

Keywords:
Machining; Chatter detection; Machining stability; Time-domain simulation; Early detection; Dynamic system supervision; Self-excited vibrations

1. INTRODUCTION

In industry, chatter avoidance is still achieved through a costly trial-and-error loop—incremental test cuts, surface inspection and parameter retuning—that can consume hours of machine time; operators therefore seek methods that predict unstable zones before, if possible, the first chip is made.

Regenerative chatter is a self-excited vibration that arises at the cutting interface and jeopardises surface integrity, tool life and productivity [Jin and Poudel, 2015]. Because the oscillation feeds on itself through the wavy surface left by the preceding tooth passage, it can amplify rapidly and force costly machine stops [Najafi and Hakim, 1992]. Although fully developed chatter is easy to recognise in sound and spindle-current signals, warning of its onset remains challenging [Kakinuma et al., 2014]. Timely alarms would avoid scrap and unplanned downtimes [Bayly et al., 2002].

Two categories of chatter are usually distinguished. Primary chatter stems from frictional, modal-coupling or thermal mechanisms [Wiercigroch and Krivtsov, 2001]; regenerative chatter, by contrast, is driven by the periodic recutting of a modulated surface and represents the dominant limit to material-removal rate in turning [Insperger and Stepán, 2000]. Classic cutting tests by Taylor laid the groundwork which led to stability charts [Taylor, 1906], while Tlusty and Polacek formalised the stability boundary, later revisited in analytical form by Altintas and Budak [Altintas and Budak, 1995]. The resulting Stability Lobe Diagram (SLD) remains the principal preventive tool, mapping stable and unstable regions versus spindle speed and depth of cut [Fu et al., 2016]. However, SLDs are computed off-line from modal tests, so any change in stiffness, mass or damping—due to tool wear, thermal drift or fixture variation—can invalidate them [Delio et al., 1992]. Tools and workpieces with low rigidity, such as Ti–Ni alloys encountered in aerospace parts, exacerbate the problem [Zou et al., 2021].

Wavelet filtering enhances transient burst detection, while Empirical Mode Decomposition isolates low-energy precursors otherwise hidden in broadband noise [Altintas and Chan, 1992]. Simulations that couple tool–workpiece dynamics with cutting-force models provide a test-bed for evaluating candidate indicators under controlled transitions between stable and unstable regimes [Li and Li, 2000]. Benchmarks show that plotting these indicators against the evolving SLD yields reliable early warnings and guides spindle-speed adjustments without interrupting production [Fu et al., 2016].

Traditional chatter detection relies on amplitude thresholds or frequency analysis, but these methods struggle with early instability detection due to discretization errors and transient fluctuations. To address this, we propose a criterion based on an energetic analysis deduced from areas computation on the trajectory in the displacement-velocity phase plane. This will allow to detect subtle energy variation before visible amplitude growth. If other authors have

already used the phase plane to analyze the stability of machining systems [Deshpande and Fofana, 2001][Wu et al., 2016], they do not use these area calculations allowing an energetic analysis. By segmenting the signal using sliding time windows, oscillatory cycles are isolated, and geometric metrics are extracted to quantify the system-s energy state. These metrics underpin a threshold-based criterion aimed at anticipating instability before amplitude growth is evident.

The paper is structured as follows: Section 2 defines the proposed indicator and details its construction. Section 3 describes the test case used to illustrate the behaviour of this criterion. The numerical modelling of this example is also given in this section. Section 4 analyzes indicator evolution for the chosen test case while section 5 concludes with key findings and future directions.

2. PROPOSED INDICATOR

The proposed indicator uses time series of displacements $x(t)$ and velocities $\dot{x}(t)$ extracted from time domain signals. Instead of tracking amplitude fluctuations, we calculate the area A of each oscillatory loop in the phase plane as a geometric proxy for dissipated energy. By continuously tracking $A(t)$, one observes their exponential growth or decay as the system departs from or returns to stability.

2.1. Phase-Diagram Construction

The phase diagram is built from the time evolution of displacement $x(t)$ and velocity $\dot{x}(t)$, yielding a trajectory

$$\mathscr{T} = \{\tau_i = (x(t_i), \dot{x}(t_i)) \mid t_i \in \mathbf{t}\}\,, \quad \mathscr{T} \in \mathbb{R}^{n\times 2}, \quad (2.1)$$

where $\mathbf{t}$ it the time interval of the machining operation.

Unlike conservative systems that produce closed orbits, these trajectories form converging or diverging spirals around a moving equilibrium, reflecting non-conservative effects such as energy dissipation or accumulation.

2.2. Sliding Time Windowing

The simulated trajectory $\mathscr{T}$ is segmented into successive windows to monitor the system's local dynamics in real time. This time-resolved framework circumvents the limitations of peak-based methods, which are prone to discretization errors and may overlook the gradual evolution of oscillatory behavior indicative of impending instability.

Window definition

Each window k is the closed interval

$$\mathscr{W}^{(k)} := \left[t_0^{(k)},\, t_0^{(k)} + \Delta T^{(k)} \geq \alpha\, T_N\right], \quad (2.2)$$

where T_N is a characteristic period of the system, and $\alpha \in \mathbb{N}^+$ denotes the number of periods to be covered. The window slides across the signal with a fixed time step Δt_{win}, following:

$$t_0^{(k)} = t_1 + k\,\Delta t_{\text{win}}, \quad k = 0, 1, 2, \ldots \quad (2.3)$$

The corresponding segment of the trajectory, defining a local sub-trajectory, is:

$$\mathscr{T}^{(k)} = \left\{\tau_i \in \mathscr{T} \,\middle|\, t_i \in \mathscr{W}^{(k)}\right\}. \quad (2.4)$$

Complete oscillations

Each window $\mathscr{W}^{(k)}$ contains a set of spiral-like dynamic cycles, referred to as complete oscillations. A complete oscillation j is defined as an ordered subset:

$$\Gamma_j^{(k)} = \left\{\tau_{i_j} = (x(t_{i_j}),\, \dot{x}(t_{i_j})) \in \mathscr{T}^{(k)}\right\}, \quad j = 1, \ldots, N_{\text{osc}}^{(k)}. \quad (2.5)$$

Series of spiral areas

Each complete oscillation yields a corresponding spiral area $A_j^{(k)}$. The set of areas within window k is denoted:

$$\boldsymbol{\mathcal{A}}^{(k)} := \left\{A_j^{(k)} \in \mathbb{R}^+ \,\middle|\, j = 1, \ldots, N_{\text{osc}}^{(k)}\right\}. \quad (2.6)$$

This sliding-window framework offers a high-resolution, cycle-by-cycle view of the system's dynamic evolution, laying the groundwork for robust detection of transitions toward instability.

2.3. Spiral Area Extraction

For each complete oscillation $\Gamma_j^{(k)} \subset \mathscr{T}^{(k)}$ in a dissipative dynamical system, we use the enclosed area in the phase plane $(x, \dot{x})$ as a geometric proxy for the mechanical energy exchanged (and lost) over one cycle.

To compute this area in a computationally efficient way, we invoke *Green's theorem*, which allows transforming a double integral over a domain into a line integral around its boundary. This not only simplifies the calculation but naturally reveals a direct link between the trajectory geometry and energy variation—especially useful in systems with closed or nearly closed orbits.

Green-theorem formulation

The Green's theorem applied around the closed trajectory $\Gamma_j^{(k)}$ gives:

$$A_j^{(k)} = \oint_{\Gamma_j^{(k)}} \vec{\psi} \cdot d\vec{r} = \iint_{\mathcal{D}} \left(\frac{\partial R}{\partial x} - \frac{\partial Q}{\partial \dot{x}}\right) dx\, d\dot{x}, \quad (2.7)$$

where $\vec{\psi} = (Q, R)$. By choosing the vector field $\psi(x, \dot{x}) = \left(-\frac{\dot{x}}{2},\, \frac{x}{2}\right)$, one finds that the curl of ψ is unity.

$$A_j^{(k)} = \oint_{\Gamma_j^{(k)}} \vec{\psi} \cdot d\vec{r} = \frac{1}{2} \oint_{\Gamma_j^{(k)}} \left(x\, d\dot{x} - \dot{x}\, dx\right). \quad (2.8)$$

Time-Domain and Discrete Approaches

Rewriting this line integral as a time integral over one oscillation—between two successive instants $t_{j,k}^{\downarrow}$ and $t_{j,k}^{\uparrow}$, corresponding to the two successive times where the sign of $\dot{x}$ goes from negative to positive. This instants can be seen on Fig. 1. Thus, (2.8) leads to:

$$A_j^{(k)} = \frac{1}{2} \int_{t_{j,k}^{\downarrow}}^{t_{j,k}^{\uparrow}} \left(x(t)\, \ddot{x}(t) - \dot{x}(t)^2\right) dt. \quad (2.9)$$

This ensures that the area estimation remains intrinsically tied to the mechanical activity internal to the cycle. For numerical implementation, the same area is robustly approximated via a simple polygonal sum over sampled $(x_i, \dot{x}_i)$ pairs:

$$A_j^{(k)} = \frac{1}{2} \sum_{l=1}^{N_{\text{osc}}^{(k)}-1} \left(x_{i_l}\, \dot{x}_{i_{l+1}} - x_{i_{l+1}}\, \dot{x}_{i_l}\right). \quad (2.10)$$

This discrete form is both efficient and accurate, enabling cycle-by-cycle quantification of energy dissipation.

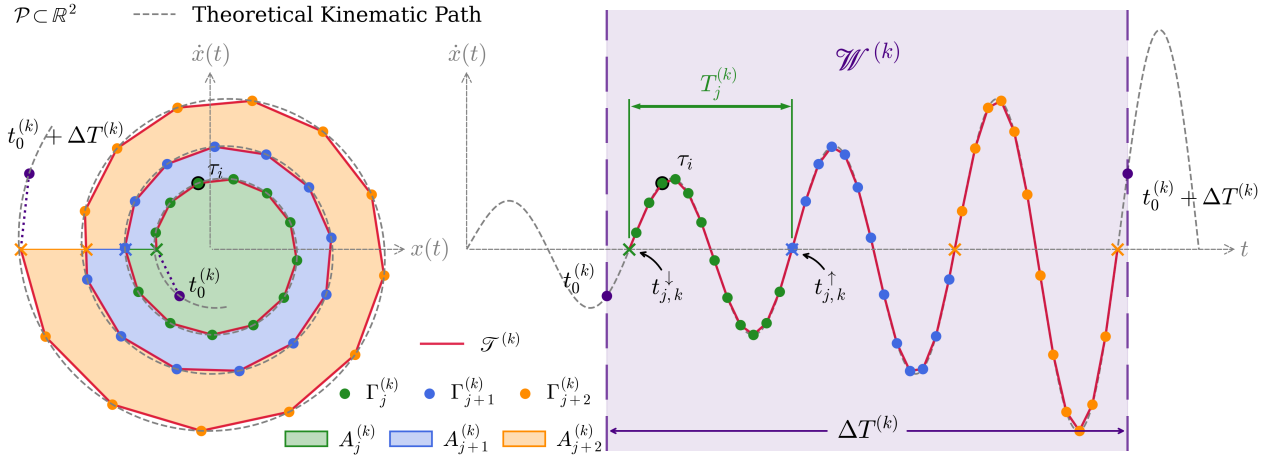

Fig. 1. *Geometric construction of the spiral-area indicator. Left: tool-tip trajectory in the displacement-velocity phase plane $\mathcal{P}$. A sliding time window $\mathcal{W}^{(k)}$ (shaded purple, right) encloses n samples from $t_0^{(k)}$ to $t_0^{(k)} + \Delta T^{(k)}$. Within the window, the trajectory $\mathscr{T}^{(k)}$ (red line) is partitioned into successive spiral cycles $\Gamma_j^{(k)}, \Gamma_{j+1}^{(k)}, \Gamma_{j+2}^{(k)}$ (green, blue, and orange markers). The oriented area of each cycle, $A_j^{(k)}, A_{j+1}^{(k)}, A_{j+2}^{(k)}$ (corresponding coloured polygons). Dashed grey curve: ideal kinematic path for reference.*

2.4. Energetic Interpretation of the Spiral Area

The spiral area $A_j^{(k)}$ associated with a complete cycle $\Gamma_j^{(k)}$ in the $(x, \dot{x})$ plane admits the exact expression

$$A_j^{(k)} = \frac{1}{2}\left[x\,\dot{x}\right]_{t_{j,k}^{\downarrow}}^{t_{j,k}^{\uparrow}} - \int_{t_{j,k}^{\downarrow}}^{t_{j,k}^{\uparrow}} \dot{x}(t)^2\,dt. \tag{2.11}$$

As at $t_{j,k}^{\downarrow}$ and $t_{j,k}^{\uparrow}$ the velocity $\dot{x}$ is null, previous equation becomes:

$$A_j^{(k)} = -\int_{t_{j,k}^{\downarrow}}^{t_{j,k}^{\uparrow}} \dot{x}(t)^2\,dt. \tag{2.12}$$

Energy balance

Starting from the equation of motion

$$m\ddot{x} + c\dot{x} + kx = F(t), \tag{2.13}$$

the mechanical-energy balance over the same interval $[t_{j,k}^{\downarrow},\, t_{j,k}^{\uparrow}]$ can be written as

$$c\int \dot{x}^2\,dt = W_{\text{ext}}^{(j,k)} - \Delta E_m^{(j,k)}, \tag{2.14}$$

where $W_{\text{ext}}^{(j,k)}$ is the external work done on the system and $\Delta E_m^{(j,k)}$ the change in mechanical energy.

Substituting this result into the area formula yields

$$c\,A_j^{(k)} = -W_{\text{ext}}^{(j,k)} + \Delta E_m^{(j,k)} \tag{2.15}$$

showing that $A_j^{(k)}$ is directly proportional, thanks to the damping coefficient, to the energy dissipated in the cycle. This established the connection between spiral geometry and energetic loss.

2.5. Extraction of Dynamic Indicators $\delta_j^{(k)}$

Local logarithmic decrement $\delta_j^{(k)}$

Given two successive spiral cycles $\Gamma_j^{(k)}$ and $\Gamma_{j+1}^{(k)}$, we define the area ratio and the local logarithmic decrement

$$r_j^{(k)} := \frac{A_{j+1}^{(k)}}{A_j^{(k)}}, \qquad \delta_j^{(k)} := -\ln r_j^{(k)}. \tag{2.16}$$

Because the spiral area A is proportional to the mechanical energy dissipated in a cycle, $\delta_j^{(k)}$ quantifies, cycle-by-cycle, the exponential evolution of this energy:

- $\delta_j^{(k)} > 0 \quad \rightarrow$ exponential decay of area and amplitude $\rightarrow$ locally damped motion.
- $\delta_j^{(k)} < 0 \quad \rightarrow$ exponential growth of area and amplitude $\rightarrow$ onset of regenerative chatter.

Relation to the local growth exponent $\lambda_j^{(k)}$

Let $T_j^{(k)} = t_{j+1,k}^{\downarrow} - t_{j,k}^{\downarrow}$ be the duration of cycle j. Assuming the area evolves exponentially,

$$A_{j+1}^{(k)} = A_j^{(k)}\, e^{\lambda_j^{(k)} T_j^{(k)}},\ \lambda_j^{(k)} := \frac{1}{T_j^{(k)}} \ln\left(\frac{A_{j+1}^{(k)}}{A_j^{(k)}}\right) \tag{2.17}$$

so that

$$\lambda_j^{(k)} = -\frac{\delta_j^{(k)}}{T_j^{(k)}} \tag{2.18}$$

and, for $T_j^{(k)} \approx T_N$ regimes,

$$\lambda_j^{(k)} \approx -\frac{\delta_j^{(k)}}{T_N}. \tag{2.19}$$

Thus $\lambda_j^{(k)}$ gives the instantaneous exponential growth rate of the spiral area. Tab. 1 gives an interpretation of $\delta_j^{(k)}$ and $\lambda_j^{(k)}$ in terms of system behavior.

$\delta_j^{(k)}$	$\lambda_j^{(k)}$	Interpretation
> 0	< 0	Damped (energy decrease)
$= 0$	$= 0$	Conservative (neutral)
< 0	> 0	Amplified (instability onset)

Table 1. *Interpretation of $\delta_j^{(k)}$ and $\lambda_j^{(k)}$ in terms of system behavior.*

Two consecutive cycles are sufficient to compute $\delta_j^{(k)}$ and $\lambda_j^{(k)}$, providing a local, real-time indicator of energy build-up or dissipation without global curve fitting.

The use of large window (with more than two cycles) may improve robustness against transient noise as this allows the analysis of an average evolution of indicators over several cycles. The choice of the number of cycles is a parameter. However, it must remain small for rapid detection of the evolution of the system.

3. SIMULATED MODEL DESCRIPTION

A classical two-degree-of-freedom (2-DOF) orthogonal cutting model, after Altintas [Altintas, 2012], is used to generate the time-domain simulations and the Stability Lobe Diagrams (SLD). Figure 2 sketches the arrangement.

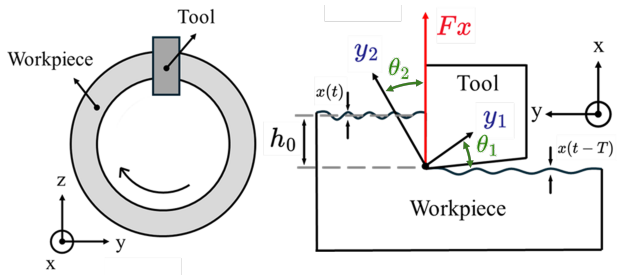

Fig. 2. *Two-degrees-of-freedom (2-DOF) system for dynamic simulations, used to generate Stability Lobe Diagrams (SLD).*

Dynamic parameters

Mode	ω_n (Hz)	ζ (%)	k (N/m)	m (kg)	θ (degree)
y_1	250	1.2	2.26×10^8	9.57	30°
y_2	150	1.0	2.13×10^8	15.48	60°

Table 2. *Modal data of the simulated system*

Cutting force and chip thickness

$$F_x(t) = K_f\, a\, h(t),\ h(t) = h_0 + x(t) - x(t-T) \quad (3.1)$$

with cutting constant $K_f = 1{,}000$ MPa, axial depth of cut a, nominal chip thickness h_0, and time delay T linked to spindle speed.

Equations of motion

For each modal direction $i \in \{1, 2\}$:

$$m_i\ddot{x}_i + c_i\dot{x}_i + k_i x_i = F_{ix}(t) \quad (3.2)$$

where F_{ix} is the projection of the cutting force on mode i.

This compact formulation retains all information required to reproduce the simulated responses and to build the corresponding SLDs while minimizing textual overhead.

Simulation Protocol

To evaluate the behavior of the proposed indicators under different dynamic conditions, two simulation cases were extracted from the Stability Lobe Diagram (SLD), all at a fixed spindle speed of 12,000 rev/min. Each case corresponds to a different axial depth of cut:

- **Case A:** $h_0 = 5$ mm (nominally stable)
- **Case B:** $h_0 = 25$ mm (fully unstable)

The generation of the time series of displacements and velocities were carried out with the *nessy2m* software [Coffignal and Lorong, 2003]. This software allows high-fidelity time-domain simulations taking into account nonlinear kinematics. Each simulation was run with a temporal resolution of $\Delta t = 10^{-4}$ s. The observable signal was the modal displacement $x(t)$, from which the phase trajectory $(x(t), \dot{x}(t))$ was constructed. The system has been reduced to the single fist eigenmode (Tab. 2).

The trajectory was segmented using the sliding window framework described in Section 2.2, with the following parameters:

- Time increment between two consecutive sliding windows: $\Delta t_{\text{win}} = 10^{-3}$ s
- Number of spiral cycles per window: $N_{\text{osc}}^{(k)} = 2$

Each complete oscillation detected within a window was processed to extract the spiral area $A_j^{(k)}$ and the associated dynamic indicators $\delta_j^{(k)}$ and $\lambda_j^{(k)}$.

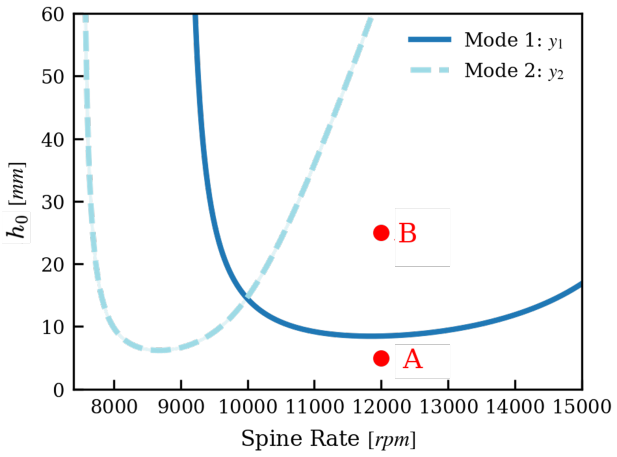

Fig. 3. *Stability Lobe Diagram (SLD) with test cases A-B.*

4. RESULTS AND DISCUSSIONS

4.1. Stability Landscape and Reference Diagram

Figure 3 shows the Stability Lobe Diagram (SLD) for the simulated system, with two selected test points (A-B) at a fixed spindle speed of 12,000 rev/min. These points serve as references for the evaluation of the proposed indicators in the next sections.

4.2. Indicator Evolution Across Regimes

Case A: Stable regime

Figure 4 shows the displacement signal $x(t)$ (blue line) and the window-level logarithmic decrement $\delta^{(k)}$ (red dots) for Case A ($h_0 = 5$ mm). The horizontal dashed line at $\delta = 0$ marks our practical threshold for chatter risk.

The initial penetration of the tool in the material generates a transient which means that the system, although stable, presents maximum vibrations of the order of 0.45 microns at the start of machining. As this entering is smooth the observed initial vibration is quite small. The system then oscillates around its equilibrium position corresponding to a constant applied cutting force and constant tool deflection (7.71 microns).

- **Signal behavior:** $x(t)$ exhibits decaying oscillations.
- **Indicator evolution:** All values of $\delta^{(k)}$ remain above the threshold ($\delta^{(k)} > 0$), indicating net energy dissipation in each cycle.
- **Interpretation:** Rather than diagnosing chatter *after* it appears, $\delta^{(k)}$ assesses the *future risk* of self-excited vibration. In Case A, $\delta^{(k)} > 0$ throughout the run implies that chatter will *not* develop under these cutting conditions.

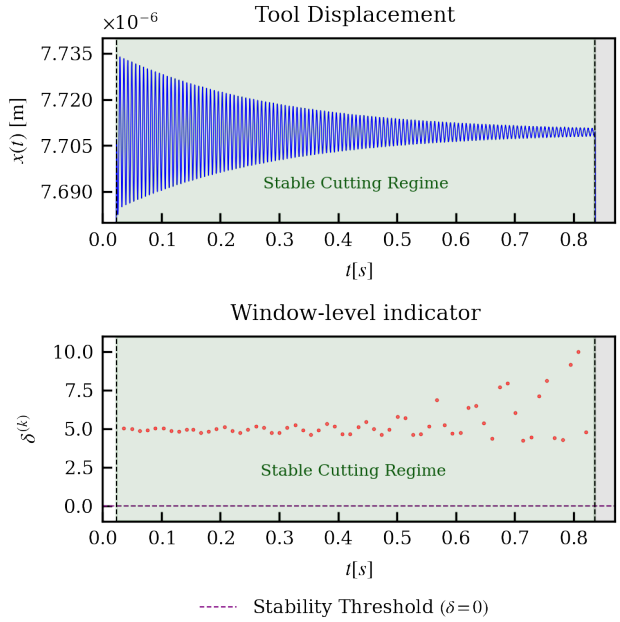

Fig. 4. *Displacement signal $x(t)$ and window-level logarithmic decrement $\delta^{(k)}$ for Case A ($h_0 = 5\,\mathrm{mm}$). The dashed line at $\delta = 0$ indicates the chatter risk threshold.*

Case B: Fully unstable regime

On Fig. 5 the blue curve shows the displacement signal $x(t)$, while red dots correspond to the logarithmic decrement $\delta^{(k)}$ computed over sliding windows. The dashed purple line at $\delta^{(k)} = 0$ marks the new detection threshold.

On this figure, the displacement evolution illustrates a dynamic-transition scenario—from quite small initial vibration ($t < 0.3$ s) to large vibration (0.5 s $< t < 0.83$ s), and back with decreasing vibration (0.83 s $< t$).

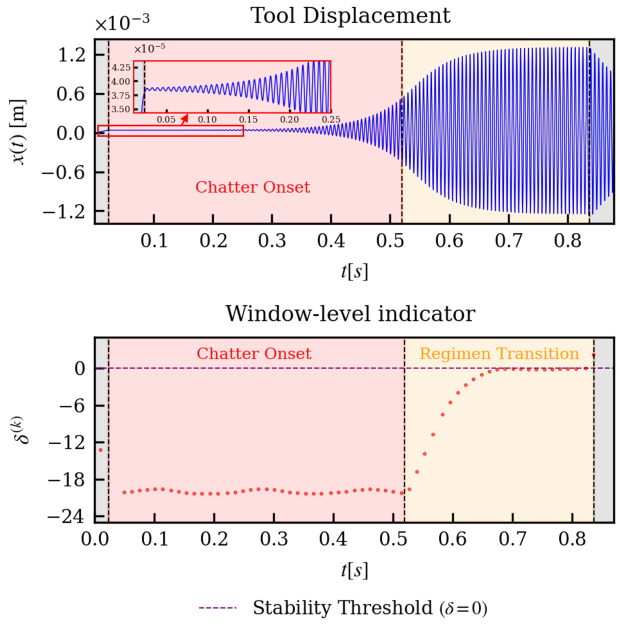

Fig. 5. *Displacement signal $x(t)$ and window-level logarithmic decrement $\delta^{(k)}$ for Case B ($h_0 = 25\,\mathrm{mm}$). The dashed line at $\delta = 0$ indicates the chatter risk threshold.*

The background is segmented into three color-coded zones, corresponding to the indicator's output:

- **Instability risk zone (red):**
  At the beginning of the machining $\delta^{(k)}$ becomes negative. The first vertical dashed line marks the start of this zone, where sustained negative values signal a net energy gain per cycle. The zoom, visible at the top of figure 5, shows that the vibrations, associated with chattering, increase as soon as the tool is in the material.
- **Steadying zone (orange):**
  The second vertical dashed line marks the return of $\delta^{(k)}$ above zero. This indicates a re-stabilization of the process and a retreat from chatter-prone conditions. This corresponds in our case, to machining condition where the tool outputs the material and leading to discontinuous cutting force.
- **Decreasing zone (gray):**
  It appears at the end of machining and when tool is outside the material and corresponds to free decreasing vibration.

4.3. Summary of Findings

The results obtained for the two A and B cases confirms that our geometric-energetic indicator provides an early, predictive measure of process stability. On B case, the indicator $\delta^{(k)}$ detects the instability at the very early apparition and before it is observable in $x(t)$. It also signals when the system exits that risk region.

The behaviour observed clarifies how the geometric–energetic framework translates phase–space dynamics into a single, actionable metric. When the system operates under the stability lobes (Case A), every spiral loop shrinks, the spiral area decays exponentially, and the window-level decrement remains strictly positive. This corresponds to a decreasing of the dissipated energy related to vibration reduction.

When the cutting parameters correspond to an operating point inside the unstable region of the SLD (Case B), the spiral area expands. The red area (Fig. 5), in which $\delta^{(k)} < 0$, marks that the dissipated energy increases and where energy injected by the cutting process surpasses energy dissipated by structural damping—a necessary and sufficient condition for chatter to emerge. The early detection offers a temporal buffer for corrective action.

These experiments demonstrate that the logarithmic decrement condenses complex, non-linear dynamics into a model-agnostic scalar that (i) discriminates stable from unstable regimes, (ii) provides an early-warning horizon determined by the window length, and (iii) tracks recovery without re-tuning. Its threshold can be calibrated once per machine and reused across operations, making it suitable for on-board implementation in adaptive control or operator-assist dashboards. The sign change of $\delta^{(k)}$ marks the moment when energy injected per cycle exceeds structural damping, providing a clear boundary between dissipative and self-excited behaviour. The indicator is obtained from a single kinematic channel and requires no offline modal identification, making it attractive for on-machine implementation.

Current ongoing work presents nevertheless many limitations:

- Real cutting environments introduce noise, sensor noise, spindle run-out and thermal drift that can mask the small spiral areas observed in marginal regimes.
- Multiple degrees of freedom systems must be studied.
- The indicator reflects a *trend* (tendency toward or away from instability). To decide whether the current vibration level is already unacceptable for part quality, additional criteria—e.g., broadband force energy or surface-finish feedback—remain necessary, vibraton amplitude.
- Generally, during industrial machining, cutting condition changes. It is quite important to test the relevance of our indicator when cutting conditions vary and are close the instability region boundary in SLD.

5. CONCLUSIONS AND PERSPECTIVES

This study has shown that the spiral-area framework converts the displacement–velocity trajectory of a cutting tool into an energy-based indicator capable of anticipating regenerative chatter. Among the metrics derived from the spiral area, the window-level logarithmic decrement $\delta^{(k)}$ offers the simplest and most consistent early-warning signal: it remains positive in stable operation and becomes persistently negative well before chatter manifests in the raw displacement.

By condensing complex phase-space dynamics into a single, physically interpretable scalar, the spiral-area decrement offers a practical path toward real-time, self-optimising machining systems that can predict—and ultimately prevent—chatter.

References

Altintas, Y. (2012). *Metal Cutting Mechanics, Machine Tool Vibrations, and CNC Design*. Cambridge University Press, 2nd edition.

Altintas, Y. and Budak, E. (1995). Analytical prediction of stability lobes in milling. *CIRP Annals*, 44(1):357–362.

Altintas, Y. and Chan, P. (1992). In-process detection and suppression of chatter in milling. *International Journal of Machine Tools and Manufacture*, 32(3):329–347.

Bayly, P., Schmitz, T., Stepan, G., Mann, B., Peters, D., and Insperger, T. (2002). Effects of radial immersion and cutting direction on chatter instability in end-milling. *ASME Manufacturing Engineering Division*, 13:351–363.

Coffignal, G. and Lorong, P. (2003). Nessy: un Logiciel éléments finis pour développer et capitaliser des travaux de recherche. In *6e Colloque National en Calcul des Structures*, Giens, France.

Delio, T., Tlusty, J., and Smith, S. (1992). Use of audio signals for chatter detection and control. *ASME Journal of Engineering for Industry*, 114(2):146–157.

Deshpande, N. and Fofana, M. S. (2001). Nonlinear regenerative chatter in turning. *Robotics and Computer-Integrated Manufacturing*, 17(1–2):107–112.

Fu, Y., Zhang, Y., Zhou, H., Li, D., Liu, H., Qiao, H., and Wang, X. (2016). Timely online chatter detection in end milling process. *Mechanical Systems and Signal Processing*, 75:668–688.

Insperger, T. and Stepán, G. (2000). Stability of the milling process. *Periodica Polytechnica Mechanical Engineering*, 44(1):47–57.

Jin, X. and Poudel, A. (2015). Experimental study on high frequency chatter attenuation in 2-d vibration assisted micro milling process. *Journal of Vibroengineering*, 17(6):2743–2754.

Kakinuma, Y., Enomoto, K., Hirano, T., and Ohnishi, K. (2014). Active chatter suppression in turning by band-limited force control. *CIRP Annals*, 63:365–368.

Li, H. and Li, X. (2000). Modeling and simulation of chatter in milling using a predictive force model. *International Journal of Machine Tools and Manufacture*, 40:2047–2071.

Najafi, B. and Hakim, H. (1992). A comparative study of nonparametric spectral estimators for application in machining vibration analysis. *Mechanical Systems and Signal Processing*, 6:551–574.

Taylor, F. (1906). *On the art of cutting metals*. American Society of Mechanical Engineers.

Wiercigroch, M. and Krivtsov, A. (2001). Frictional chatter in orthogonal metal cutting. *Philosophical Transactions of the Royal Society of London*, 359(A):713–738.

Wu, S., Li, R., Liu, X., Yang, L., and Zhu, M. (2016). Experimental study of thin wall milling chatter stability nonlinear criterion. *Procedia CIRP*, 56:422–427.

Zou, P., Wang, H., Zheng, C., Hu, L., Chang, J., and Wei, B. (2021). Electrostatic levitation processing and microscopic hardness property of hyperperitectic ti60ni40 alloy. *Intermetallics*, 130:106934.